machines

MDPI

Article

MTPA Control for IPMSM Drives Based on Pseudorandom Frequency-Switching Sinusoidal Signal Injection

Ke Li [1], Tianfu Sun [1,2], Fucheng Jiang [1], Wei Feng [1,*] and Huiyun Li [1]

[1] Shenzhen Institute of Advanced Technology, Chinese Academy of Sciences, Shenzhen 518055, China; ke.li1@siat.ac.cn (K.L.); tf.sun@siat.ac.cn (T.S.); fc.jiang@siat.ac.cn (F.J.); hy.li@siat.ac.cn (H.L.)
[2] CAS Key Laboratory of Human-Machine Intelligence-Synergy Systems, Shenzhen Institute of Advanced Technology, Shenzhen 518055, China
* Correspondence: wei.feng@siat.ac.cn

Abstract: Among various maximum torque per ampere (MTPA) control schemes for interior permanent magnet synchronous motor (IPMSM) drives, the signal-injection-based methods exhibit relatively high overall performance due to their high control accuracy and satisfactory dynamic performance. However, the high current spectrum peaks induced by the fixed-frequency signal injection may cause electromagnetic interference and even audible noise problems in applications, such as electric vehicles, vessels, and aircraft. To address this problem, an MTPA control method using pseudorandom frequency-switching sinusoidal signal injection is proposed in this paper. The sinusoidal signals with two different frequencies are randomly injected into the *d*- and *q*-axis currents and the MTPA points can be tracked according to the resultant system response. In this way, a high-performance MTPA control can be achieved regardless of motor parameter variations. Since the injection frequency of the proposed method varies randomly, the induced harmonic components in phase currents no longer concentrate at certain frequencies, and the current spectrum peaks caused by signal injection can be reduced accordingly. The experimental results demonstrate the validity of the presented method.

Keywords: interior permanent magnet synchronous motor (IPMSM); motor and drive losses; maximum torque per ampere (MTPA) control; motor parameter variations; pseudorandom frequency-switching (PRFS) signal injection

check for updates

Citation: Li, K.; Sun, T.; Jiang, F.; Feng, W.; Li, H. MTPA Control for IPMSM Drives Based on Pseudorandom Frequency-Switching Sinusoidal Signal Injection. *Machines* **2022**, *10*, 231. https://doi.org/10.3390/machines10040231

Academic Editor: Antonio J. Marques Cardoso

Received: 25 February 2022
Accepted: 22 March 2022
Published: 25 March 2022

Publisher's Note: MDPI stays neutral with regard to jurisdictional claims in published maps and institutional affiliations.

Copyright: © 2022 by the authors. Licensee MDPI, Basel, Switzerland. This article is an open access article distributed under the terms and conditions of the Creative Commons Attribution (CC BY) license (https://creativecommons.org/licenses/by/4.0/).

1. Introduction

Permanent magnet synchronous motors (PMSMs) are well known for their high efficiency, high power density, high torque to inertia ratio, etc [1,2]. Interior PMSMs (IPMSMs), as a special kind of PMSMs, also have the advantages of robust rotor structure and strong flux weakening capability, and thus are being increasingly applied in electric vehicles. For an IPMSM, both the alignment torque and reluctance torque can be generated, and a proper current control strategy is required to distribute the *d*- and *q*-axis currents. Among current control strategies, such as maximum efficiency per ampere control [3], loss minimization control [4], and maximum torque per ampere (MTPA) control [5], the MTPA control is the most widely adopted choice. With this strategy, the required torque can be generated with the minimum current magnitude, and hence the losses of both the IPMSM and its drive can be effectively reduced.

It is well known that MTPA control is closely related to multiple motor parameters, and these parameters vary with the operating conditions of the motor [6,7]. To deal with this challenge, numerous MTPA control methods considering motor parameter variations have been presented, which can be divided into five categories: (1) look-up table (LUT)-based methods; (2) search-based methods; (3) equation-based methods; (4) signal-injection-based methods, and (5) virtual-signal-injection-based methods.

The LUT-based methods and the search-based methods acquire the MTPA operating points by means of offline tests (or numerical analysis) [8] and online search [9], respectively. These methods have the advantage of requiring no motor parameters, but they may suffer from some problems. For instance, the LUT-based methods are time-consuming and are unable to fully consider the motor parameter variations due to the temperature or aging effects, while the search-based methods exhibit relatively poor dynamic performance.

The equation-based methods are a type of widely applied MTPA control scheme, which uses the MTPA equation derived from the motor mathematical model to calculate the MTPA current [10] or flux [11] online. The motor parameters in the MTPA equation are usually obtained from predefined LUTs [12] or online parameter estimations [13] to cope with the influence of parameter variations. Nevertheless, most of these methods neglect the derivatives of motor parameters with respect to the current vector angle (or d- and q-axis currents), which may cause large MTPA control deviation at a high current amplitude level [14]. In Ref. [15], the derivatives of motor parameters were considered via a variable equivalent parameter. However, this method still needs to be improved to obtain the equivalent parameter completely online.

The signal-injection-based methods are a type of parameter-insensitive MTPA control scheme, which inject high-frequency (HF) signals into the motor, and then detect the MTPA points according to the resultant response of a system variable, such as torque [16], speed [17], speed regulator output [18], electric power [19], stator flux linkage [20], and dc-link current [21]. In this way, an MTPA control with high accuracy and satisfactory dynamic performance can be achieved. The existing signal-injection-based methods usually use fixed injection frequencies, and the induced HF components in phase currents concentrate at certain frequencies, resulting in high current spectrum peaks. These high current spectrum peaks induced by the injected HF signals may cause electromagnetic interference and even audible noise problems [22], imposing a severe restriction to the widespread application of the signal-injection-based methods.

The virtual-signal-injection-based methods are a type of interesting MTPA control scheme. Instead of real injection, these methods inject HF signals into the current vector angle mathematically and then adjust the current vector according to the virtual torque response until the MTPA condition is reached [23–26]. Since this type of method requires no real-signal injection, the possible negative effects due to the injected signals can be avoided. However, the derivatives of motor parameters with respect to the current vector angle are not fully considered in these methods. Hence, like the equation-based methods, they may also suffer from the control deviation problem at high current amplitude levels. To address this problem, a virtual-signal-injection-based method with an online derivative term estimator was proposed in [27]. Unfortunately, its dynamic performance is unsatisfactory.

According to the above discussions, the signal-injection-based methods have the advantages of high control accuracy and satisfactory dynamic performance, exhibiting relatively high overall performance among different types of MTPA control schemes; however, the high current spectrum peaks due to the conventional fixed-frequency signal injection may cause negative effects in some applications.

In this paper, a novel MTPA control method based on a pseudorandom frequency-switching (PRFS) signal injection is proposed for IPMSM drives. Different from the conventional signal-injection-based methods, the injection frequency of the proposed method switches randomly between two candidate frequencies. In this way, the harmonic current will no longer concentrate at certain frequencies, and the current spectrum peaks due to the signal injection can be reduced accordingly. Moreover, the proposed method inherits the advantages of the signal-injection-based methods, and hence, it can realize a high-performance MTPA control regardless of motor parameter variations. The effectiveness of the presented method is validated by extensive experiments on an IPMSM drive system.

2. MTPA Indicator

The mathematical model of an IPMSM can be expressed in the rotor reference frame as:

$$u_d = Ri_d + L_d\frac{di_d}{dt} - p\omega_m L_q i_q \tag{1}$$

$$u_q = Ri_q + L_q\frac{di_q}{dt} + p\omega_m L_d i_d + p\omega_m \psi_f \tag{2}$$

$$T_e = \frac{3p}{2}\left[\psi_f i_q + \left(L_d - L_q\right) i_d i_q\right] \tag{3}$$

where $u_{d,q}$, $i_{d,q}$, and $L_{d,q}$ are the d- and q-axis voltages, currents, and inductances, respectively; R, ψ_f, ω_m, p, and Te are the stator resistance, permanent magnet flux linkage, mechanical angular speed, number of pole pairs, and electromagnetic torque, respectively. For a practical IPMSM, the parameters L_d, L_q, and ψ_f are usually functions of i_d and i_q due to magnetic saturation.

It can be seen from Equation (3) that, for a given torque, there can be countless combinations of i_d and i_q. Among these (i_d, i_q) combinations, the optimal combination with the minimum current magnitude is called the MTPA point. To obtain the MTPA point, the most common practice is to calculate it by substituting nominal motor parameters into the MTPA Equation (4). However, such a practice may result in large MTPA control deviation due to the neglect of motor parameter variations [14].

$$i_d = \frac{\psi_f}{2\left(L_q - L_d\right)} - \sqrt{\frac{\psi_f^2}{4\left(L_q - L_d\right)^2} + i_q^2} \tag{4}$$

In fact, the MTPA points considering motor parameter variations can be considered as solutions to the following constrained optimization problem:

$$\text{minimize } |i_s| = \sqrt{i_d^2 + i_q^2}, \text{ subject to } T_e = T_{e0} \tag{5}$$

where $|i_s|$ is the magnitude of the stator current, and T_{e0} is the desired torque. From the constrained optimization problem (5), the MTPA condition $i_d(\partial T_e/\partial i_q) - i_q(\partial T_e/\partial i_d) = 0$ can be derived using the Lagrange multiplier method. For convenience, let the left-hand side of the above MTPA condition be denoted by F, i.e.,

$$F = i_d\frac{\partial T_e}{\partial i_q} - i_q\frac{\partial T_e}{\partial i_d}. \tag{6}$$

Then, the derived MTPA condition $i_d(\partial T_e/\partial i_q) - i_q(\partial T_e/\partial i_d) = 0$ can be summarized as $F = 0$. According to [21], the schematic diagram of the typical $i_d - |i_s|$ and $i_d - F$ curves under a constant torque can be shown in Figure 1, which is helpful to understand the detailed characteristics of F. As can be seen, the characteristics of F are as follows: (1) the sign of F indicates that the operating point is located at the left or right side of the MTPA point, and $F = 0$ is satisfied at the MTPA point; (2) the value of F reflects the distance between the operating point and the MTPA point. Given these characteristics, F can serve as an MTPA indicator, and an accurate MTPA control can be achieved by forcing $F = 0$.

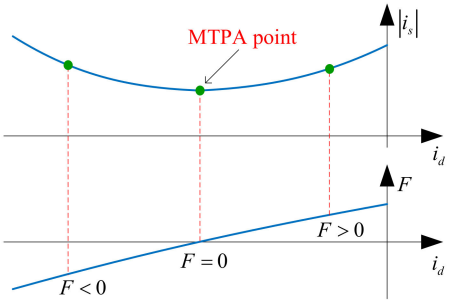


Figure 1. Schematic diagram of the typical $i_d - |i_s|$ and $i_d - F$ curves under a constant torque.

3. Proposed MTPA Control Method Based on PRFS Signal Injection

To realize a signal-injection-based MTPA operation with low injection-induced current spectrum peaks, an MTPA control method using PRFS sinusoidal signal injection is proposed in this section.

3.1. PRFS Sinusoidal Signal for Injection

As reported in [21], the HF signals injected into the d- and q-axis currents for MTPA control can be expressed as:

$$\begin{cases} i_{dh} = -i_{q0} A \sin \omega_h t \\ i_{qh} = i_{d0} A \sin \omega_h t \end{cases} \tag{7}$$

where i_{d0} and i_{q0} are the dc components of the d- and q-axis currents, respectively, and A ($0 < A < 0.08$) and ω_h are the injection gain and injection frequency, respectively.

In the conventional signal-injection-based methods, the injection frequencies are fixed, and the induced HF components in phase currents concentrate at certain frequencies, causing high current spectrum peaks. Unlike the conventional methods, the injection frequency of the proposed method is selected randomly between two candidate frequencies, so as to reduce the injection-induced current spectrum peaks.

Figure 2 shows the schematic diagram of the PRFS sinusoidal signal generation. As can be seen, N is a pseudorandom number between 0 and 1; if N = 0, the lower candidate frequency ω_{h1} is chosen as the injection frequency, otherwise, the higher candidate frequency ω_{h2} is chosen, as shown in Equation (8); after finishing a sinusoidal cycle, the pseudorandom number N is updated; by repeating the above processes, the PRFS sinusoidal signal for MTPA control can be generated. It should be noted that to make the randomly varying injection frequency switches at the zero point of the sinusoidal signal, the periods corresponding to ω_{h1} and ω_{h2} should be integral multiples of the pulse width modulation (PWM) period.

$$\omega_h = \begin{cases} \omega_{h1} & N = 0 \\ \omega_{h2} & N = 1 \end{cases} \tag{8}$$

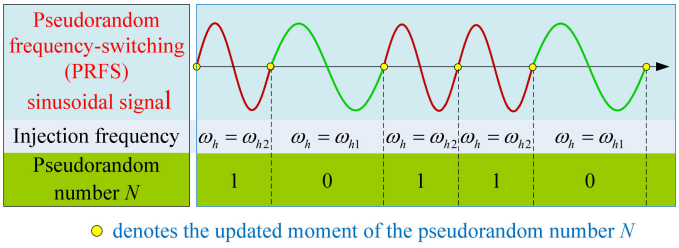


Figure 2. Schematic diagram of the PRFS sinusoidal signal generation.

In this paper, the generation of the pseudorandom number N is primarily based on the 32-bit xorshift algorithm [28] represented by:

$$\begin{cases} X = (S_{k-1} << 13) \oplus S_{k-1} \\ Y = (X >> 17) \oplus X \\ S_k = (Y << 5) \oplus Y \end{cases} \tag{9}$$

where $\oplus$ represents the bitwise XOR operator, the subscript "k" denotes the kth injection cycle, S_k is the 32-bit pseudorandom number among [1, $2^{32} - 1$] whose initial value is 2,463,534,242, and X and Y are the 32-bit intermediate variables. Then, the pseudorandom number N between 0 and 1 can be generated according to S_k as:

$$N = \begin{cases} 0 & S_k < S_p \cdot (2^{32} - 1) \\ 1 & S_k \geq S_p \cdot (2^{32} - 1) \end{cases} \tag{10}$$

where S_p is the switching probability, which is set according to Equation (11) in this paper to equalize the action time of the two candidate injection frequencies.

$$S_p = \frac{\omega_{h1}}{\omega_{h1} + \omega_{h2}} \tag{11}$$

3.2. Electric Power Response Due to Signal Injection

The electric power of the motor, i.e., P_e can be expressed as Equation (12). Based on Equations (1)–(3), Equation (12) can be rewritten as Equation (13).

$$P_e = \frac{3}{2}(u_d i_d + u_q i_q) \tag{12}$$

$$P_e = \frac{3}{2}\left[R(i_d^2 + i_q^2) + L_d i_d \frac{di_d}{dt} + L_q i_q \frac{di_q}{dt}\right] + \omega_m T_e(i_d, i_q) \tag{13}$$

It follows from Equation (7) that the d- and q-axis currents after the signal injection can be expressed as:

$$\begin{cases} i_d = i_{d0} - i_{q0} A \sin \omega_h t \\ i_q = i_{q0} + i_{d0} A \sin \omega_h t \end{cases} \tag{14}$$

Next, substituting Equation (14) into Equation (13) yields the electric power considering the signal injection, namely:

$$\begin{aligned} P_e = {} & \tfrac{3}{2}R(i_{d0}^2 + i_{q0}^2)(1 + \tfrac{1}{2}A^2) - \tfrac{3}{4}R(i_{d0}^2 + i_{q0}^2)A^2 \cos 2\omega_h t \\ & + \tfrac{3}{4}(L_d i_{q0}^2 + L_q i_{d0}^2)A^2 \omega_h \sin 2\omega_h t - \tfrac{3}{2}(L_d - L_q) i_{d0} i_{q0} A \omega_h \cos \omega_h t + \omega_m T_e(i_d, i_q) \end{aligned} \tag{15}$$

It can be observed from Equation (15) that to analyze the response of P_e due to the signal injection, specific information regarding the resultant torque $T_e(i_d, i_q)$ is required. By performing the bivariate Taylor series expansion, the resultant torque $T_e(i_d, i_q)$ can be represented as:

$$\begin{aligned} T_e(i_d, i_q) &= T_e(i_{d0} - i_{q0} A \sin \omega_h t, i_{q0} + i_{d0} A \sin \omega_h t) \\ &= T_e(i_{d0}, i_{q0}) + \left[i_{d0} \tfrac{\partial T_e}{\partial i_q}(i_{d0}, i_{q0}) - i_{q0} \tfrac{\partial T_e}{\partial i_d}(i_{d0}, i_{q0})\right] A \sin \omega_h t + \cdots \end{aligned} \tag{16}$$

In Equation (16), the term in the square bracket is actually the dc component of the MTPA indicator F shown in Equation (6), namely:

$$i_{d0} \frac{\partial T_e}{\partial i_q}(i_{d0}, i_{q0}) - i_{q0} \frac{\partial T_e}{\partial i_d}(i_{d0}, i_{q0}) = F(i_{d0}, i_{q0}) \tag{17}$$

This means that the resultant torque $T_e(i_d, i_q)$ shown in Equation (16) can be rewritten as:

$$T_e(i_d, i_q) = T_e(i_{d0}, i_{q0}) + F(i_{d0}, i_{q0}) A \sin \omega_h t + \cdots \tag{18}$$

After $T_e(i_d, i_q)$ is derived, by substituting Equation (18) into Equation (15), a more detailed expression of the electric power response due to the signal injection can be obtained as:

$$\begin{aligned} P_e = {} & \tfrac{3}{2} R (i_{d0}^2 + i_{q0}^2) \left(1 + \tfrac{1}{2} A^2\right) + \omega_m T_e(i_{d0}, i_{q0}) \\ & - \tfrac{3}{4} R (i_{d0}^2 + i_{q0}^2) A^2 \cos 2\omega_h t + \tfrac{3}{4} (L_d i_{q0}^2 + L_q i_{d0}^2) A^2 \omega_h \sin 2\omega_h t \\ & - \tfrac{3}{2} (L_d - L_q) i_{d0} i_{q0} A \omega_h \cos \omega_h t + A \omega_m F(i_{d0}, i_{q0}) \sin \omega_h t + \cdots \end{aligned} \tag{19}$$

3.3. Extraction of MTPA Indicator Information

Because the dc component of the MTPA indicator, i.e., $F(i_{d0}, i_{q0})$ indicates whether the operating point (i_{d0}, i_{q0}) is the MTPA point, it is necessary to evaluate $F(i_{d0}, i_{q0})$. As can be seen from Equation (19), $F(i_{d0},i_{q0})$ is contained in the last term of the electric power P_e, i.e., the term proportional to $\sin\omega_h t$. In this case, the information regarding $F(i_{d0},i_{q0})$ can be extracted from P_e with the demodulation technique shown in Figure 3.

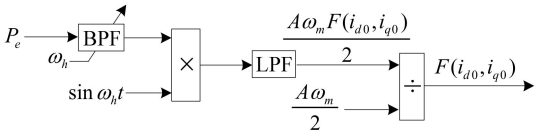


Figure 3. Demodulation technique for extracting the MTPA indicator information.

As can be seen in Figure 3, the electric power P_e is first filtered by a band-pass filter (BPF). Since the center frequency of the BPF varies with the random-injection frequency ω_h, the injection frequency component of P_e (i.e., the terms containing $\sin\omega_h t$ and $\cos\omega_h t$ in Equation (19)) can be extracted by this BPF. Then, the output of the BPF is multiplied by $\sin\omega_h t$, and the product can be represented by Equation (20). After that, this product is fed into a low-pass filter (LPF) to obtain only the dc component, i.e., the last term of Equation (20). Finally, the obtained dc component $A\omega_m F(i_{d0},i_{q0})/2$ is divided by $A\omega_m/2$, and the MTPA indicator information $F(i_{d0},i_{q0})$ can be extracted.

$$\begin{aligned} & \left[A\omega_m F(i_{d0}, i_{q0}) \sin \omega_h t - \tfrac{3}{2}(L_d - L_q) i_{d0} i_{q0} A \omega_h \cos \omega_h t\right] \cdot \sin \omega_h t \\ & = -\tfrac{3(L_d - L_q) i_{d0} i_{q0} A \omega_h}{4} \sin 2\omega_h t - \tfrac{A\omega_m F(i_{d0}, i_{q0})}{2} \cos 2\omega_h t + \tfrac{A\omega_m F(i_{d0}, i_{q0})}{2} \end{aligned} \tag{20}$$

As discussed above, the MTPA indicator information $F(i_{d0},i_{q0})$ can be extracted from the electric power P_e under the PRFS signal injection. This MTPA indicator information will be employed to adjust the operating point of the motor until it equals zero, i.e., $F(i_{d0},i_{q0}) = 0$. In this way, the motor can operate on the MTPA points.

3.4. Implementation of the Proposed MTPA Control Scheme

From the above discussions, the implementation of the proposed MTPA control scheme can be depicted in Figure 4, where the superscript "*" represents the reference value. The PRFS sinusoidal signal generation module is used to provide the desired PRFS sinusoidal signal. The injected signal references i_{dh}^* and i_{qh}^* can be calculated using Equation (7), accordingly. Then, with the help of the current control loop module, the injected signals can be injected into the d- and q-axis currents according to their references i_{dh}^* and i_{qh}^*. In this case, the MTPA indicator information $F(i_{d0},i_{q0})$ can be extracted from the electric power P_e through the MTPA indicator information extraction module, as discussed in Sections 3.2 and 3.3. Since $F(i_{d0},i_{q0})$ is equal to zero when the operating point (i_{d0}, i_{q0}) is at the MTPA point, it is employed to generate i_{d0}^* through an integrator controller with a zero

command value. In this way, $F(i_{d0},i_{q0})$ can be forced to zero, i.e., the motor can operate on the MTPA points.

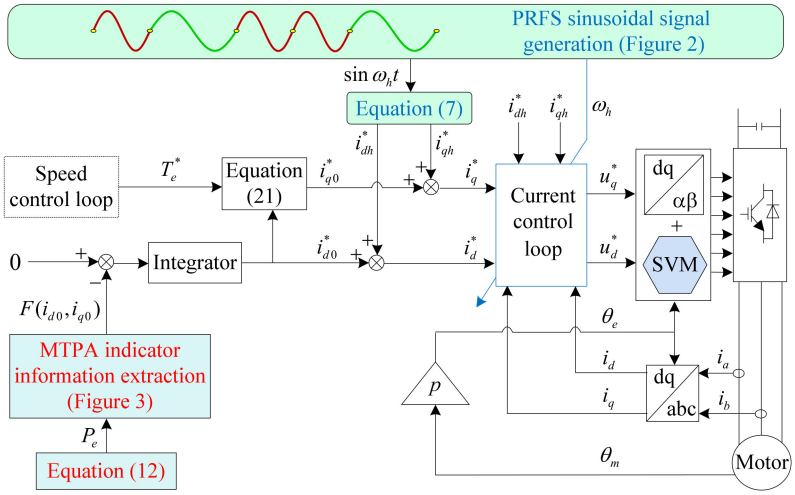


Figure 4. Block diagram of the proposed MTPA control scheme based on PRFS signal injection.

In Figure 4, the reference of the dc component of the q-axis current (namely, i_{q0}^*) is generated based on Equation (21), where the motor parameters L_d, L_q, and ψ_f can be assumed as their nominal values. The generation of the reference i_{d0}^* is independent of i_{q0}^* and Equation (21), and hence, although inaccurate motor parameters are employed in Equation (21), the accuracy of the MTPA point tracking will not be affected [14]. The adoption of inaccurate motor parameters in Equation (21) may result in torque error, which can be automatically compensated by the speed control loop.

$$i_{q0}^* = \frac{T_e^*}{\frac{3}{2}p\left[\psi_f + (L_d - L_q)i_{d0}^*\right]} \tag{21}$$

Different from the conventional signal-injection-based methods, which use fixed injection frequencies, the proposed method employs the pseudorandom-switching injection frequency, making the current harmonics no longer concentrated at certain frequencies. Hence, the proposed method can exhibit lower injection-induced current spectrum peaks compared with the conventional methods. Moreover, it can be seen from Figure 4 that the MTPA indicator information can be obtained independently of motor parameters. Thus, although the injection frequency varies randomly, the proposed method inherits the advantage of the signal-injection-based methods, i.e., being robust to motor parameter variations.

To visually demonstrate the performance of the proposed MTPA control method against motor parameter variations, Figure 5 shows the simulation results under a load torque of 30 N·m when a 20% step change is manually applied to the motor parameter ψ_f and L_q. It can be seen that although the MTPA currents changed after the step change is applied to motor parameters, the measured d- and q-axis currents can still converge to the new MTPA currents accurately. This means that the proposed method is stable under severe motor parameter variations, and the motor parameter variations have a very limited effect on the MTPA control accuracy of the proposed method.

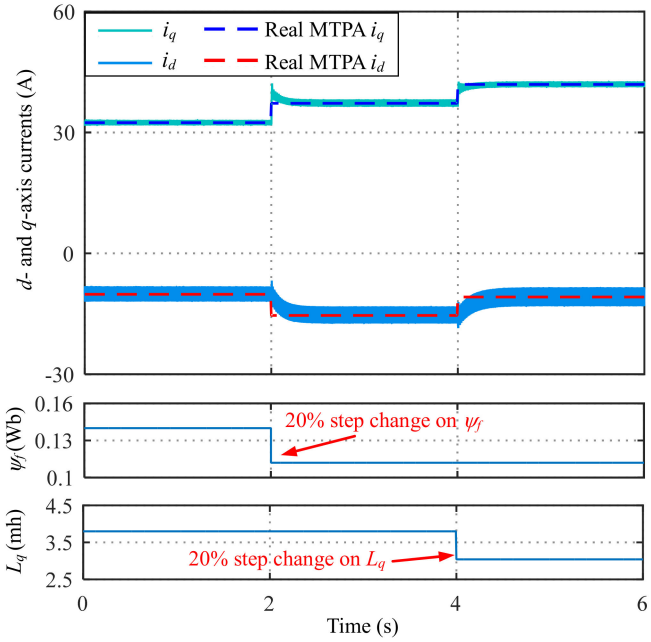


Figure 5. Simulation results of the proposed method against motor parameter variations under a load torque of 30 N·m.

3.5. Current Control Loop Considering PRFS Signal Injection

In this paper, the PRFS current signal injection is required, which needs to be realized through the current control loop. However, the conventional PI-based current control loop is not competent for this task since the injection frequency is high and pseudorandom-switching. The current control loop reported in [19] may support the changeable signal injection frequency. Nevertheless, the process variables and outputs of the two separated BPFs cannot be reasonably assigned at the frequency-switching moment, making the HF components unable to rapidly track their references after the frequency-switching, as shown in the results presented in [19]. To meet the requirement of the PRFS current signal injection, a variable-frequency BPF is used to replace the two separated BPFs of the current control loop in [19]. Then, the enhanced current control loop can be shown in Figure 6, which contains the PI-based control loop and the PRFS sinusoidal signal auxiliary control loop, allowing both the dc and randomly-injected components of the d- and q-axis currents to track their references.

It can be seen from Figure 6 that the PRFS auxiliary control loop consists of BPFs and proportional controllers. The center frequencies of the BPFs are set at the injection frequency ω_h to extract the randomly-injected components i_{dh} and i_{qh}. This makes it possible for the auxiliary control loop to regulate only the randomly-injected components with no influence on the dc components. Additionally, it can be observed from Figure 6 that the PI-based control loop also has an effect on the regulation of the randomly-injected components. This is because the inputs of the PI controllers, i.e., $i_d^* - i_d$ and $i_q^* - i_q$ contain the randomly-injected components $i_{dh}^* - i_{dh}$ and $i_{qh}^* - i_{qh}$, respectively. Considering the effects of both the PRFS sinusoidal signal auxiliary control loop and the PI-based control loop, the equivalent block diagram of the injection frequency current control loop (take the d axis as an example) can be shown in Figure 7.

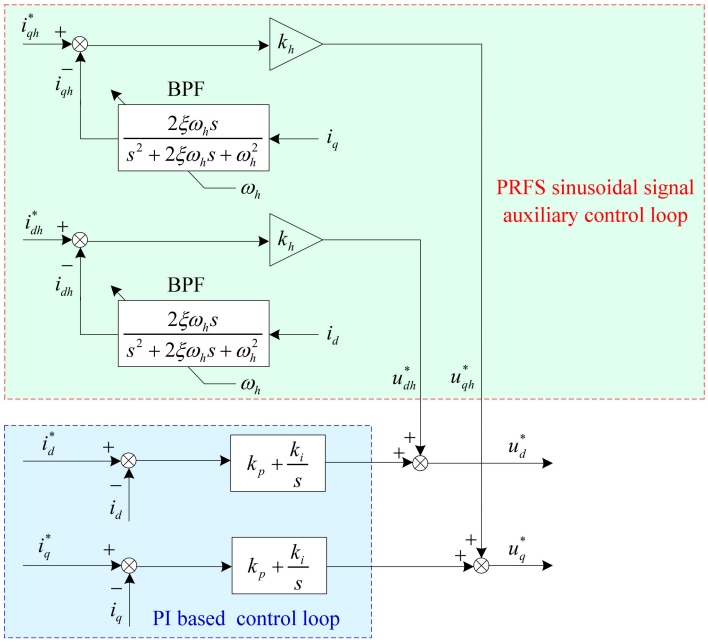


Figure 6. Enhanced current control loop considering PRFS signal injection.

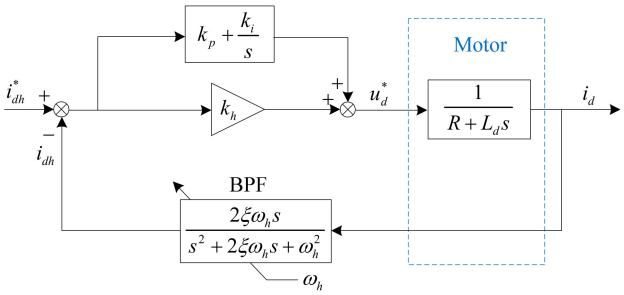


Figure 7. Equivalent block diagram of the injection frequency current control loop.

From Figure 7, the transfer function of the equivalent injection frequency current control loop can be derived as:

$$\frac{i_{dh}(s)}{i_{dh}^*(s)} = \frac{2\xi\omega_h(k_h+k_p)s + 2\xi\omega_h k_i}{L_d s^3 + (2\xi\omega_h L_d + R)s^2 + [\omega_h^2 L_d + 2\xi\omega_h(k_h+k_p) + 2\xi\omega_h R]s + \omega_h^2 R + +2\xi\omega_h k_i} \tag{22}$$

Substituting $s = j\omega_h$ into Equation (22), the frequency characteristic of Equation (22) at the injection frequency ω_h can be obtained as follows:

$$\frac{i_{dh}(j\omega_h)}{i_{dh}^*(j\omega_h)} = \frac{k_i + j\omega_h(k_h+k_p)}{k_i - \omega_h^2 L_d + j[\omega_h(k_h+k_p) + \omega_h R]} \tag{23}$$

The gain k_h of the proportional controllers in the injection frequency control loop can be designed as the value satisfying

$$\begin{cases} \omega_h(k_h+k_p) >> k_i \\ \omega_h(k_h+k_p) >> \left|(k_i - \omega_h^2 L_d) + j\omega_h R\right| \end{cases} \tag{24}$$

Then, combining Equations (23) and (24) yields Equation (25). This means that the PRFS sinusoidal reference i_{dh}^* can be accurately tracked by i_{dh}. Similarly, the PRFS sinusoidal reference i_{qh}^* can also be accurately tracked by i_{qh}. Therefore, the desired PRFS sinusoidal signals can be accurately injected into the d- and q-axis currents with the current control

loop shown in Figure 6. The PRFS sinusoidal tracking performance of the current control loop will be verified in Section 4.

$$\frac{i_{dh}(j\omega_h)}{i^*_{dh}(j\omega_h)} \approx 1 \tag{25}$$

4. Experimental Results

To experimentally evaluate the performance of the proposed MTPA control method, experiments were conducted on a prototype IPMSM drive system. The IPMSM is coaxially coupled to a dynamometer, where the dynamometer is operated in speed control mode and the tested IPMSM is operated in torque control mode. The parameters of the IPMSM are listed in Table 1. The control algorithm is implemented through dSPACE DS1202. The PWM frequency and the current sampling frequency are both 10 kHz. In the experiments, the injection gain A of the proposed method and the comparable fixed-frequency injection method are set as the same values, i.e., $A = 0.05$.

Table 1. Specification of the IPMSM.

Items	Values
Rated power	4 kW
Rated torque	38 N·m
Rated speed	1000 r/min
Rated current	40 A
Number of pole pairs	4
Stator resistance	0.08 Ω
Permanent magnet flux linkage	0.14 Wb
d-*q* axis inductances	2.3/3.8 mH

Since the PRFS sinusoidal signal injection is critical for the proposed method, the PRFS sinusoidal tracking performance of the current control loop, shown in Figure 6, was first tested. In this test, the two candidate frequencies for the PRFS sinusoidal signal injection are $\omega_{h1} = 344.83$ Hz and $\omega_{h2} = 434.78$ Hz, and the magnitudes of the references i^*_{dh} and i^*_{qh} are manually set as 1.5 and 0.5 A, respectively. Figure 8 shows the resultant PRFS sinusoidal current components and their references, as well as the relevant zoomed-in views. It can be seen that, as discussed in Section 3.5, i_{dh} and i_{qh} follow their respective references i^*_{dh} and i^*_{qh} closely. The performance of the current control loop can meet the requirements of the PRFS signal-injection-based MTPA control.

The proposed method was tested under various torque levels, and the current trajectory connected by the resultant steady-state operating points is depicted in the $|i_s| - i_d$ plane in Figure 9. For comparison, Figure 9 also shows the real MTPA current trajectory obtained by offline detection, the current trajectory based on Equation (4) using constant parameters, and the constant torque curves, where the constant torque curves from bottom to top are 5, 10, 15, 20, 30, 40, and 50 N·m, respectively. The results in Figure 9 show that the current trajectory based on Equation (4) significantly deviates from the real MTPA current trajectory, due to the neglect of motor parameter variations. By contrast, the current trajectory of the proposed scheme matches well with the real MTPA current trajectory. This demonstrates that the proposed method based on PRFS signal injection can achieve a high MTPA control accuracy.

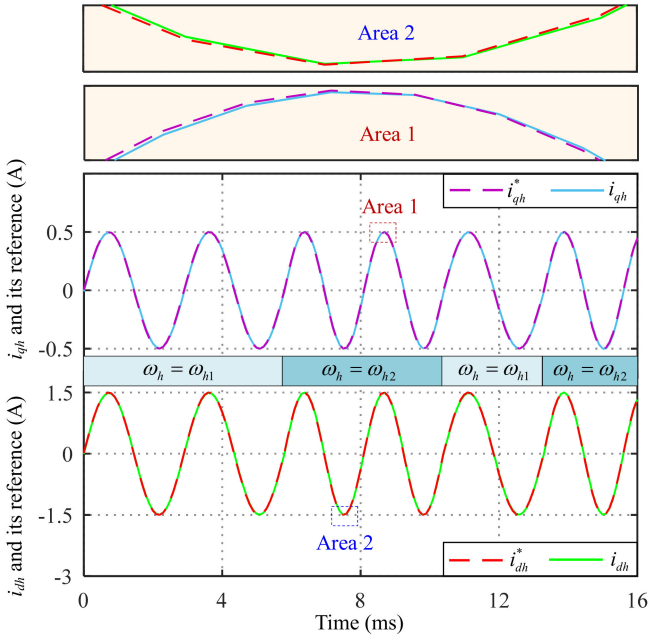


Figure 8. Results of the performance of the PRFS sinusoidal current control.

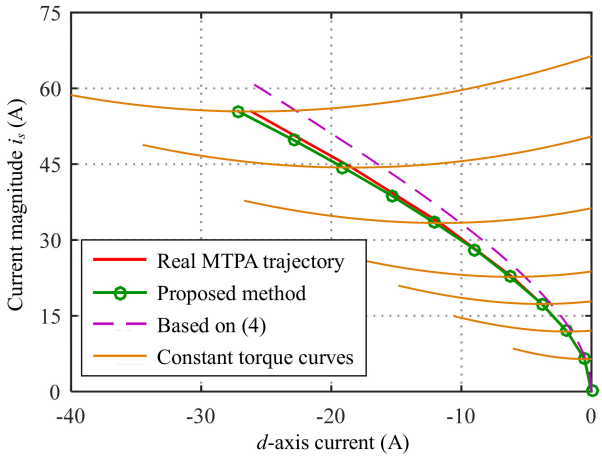


Figure 9. Experimental current trajectory of the proposed method and other comparable current trajectories.

Furthermore, the proposed method was tested at 500 r/min under a step torque of 10-30-10 N·m, and the results are shown in Figure 10. As can be seen, after the torque changed abruptly, the d- and q-axis currents were adjusted quickly until they tracked the real MTPA currents. Consequently, the proposed method can tolerate torque transients, showing high stability under severe conditions; moreover, it exhibits a satisfactory dynamic response.

The performance of the proposed PRFS injection method and the conventional fixed-frequency injection method were tested at 600 r/min under 40 N·m. Because the injection frequency of the proposed method switches between the two candidate frequencies ω_{h1} = 344.83 Hz and ω_{h2} = 434.78 Hz, the conventional fixed-frequency method was tested with these two injection frequencies, respectively, for a fair comparison. The obtained stator phase currents and their Fast Fourier Transform (FFT) results are shown in Figure 11. It can be seen from Figure 11a that with the fixed-frequency method, the phase current FFT result shows two obvious peaks at the frequency of $\omega_h \pm \omega_e$ (ω_e is the electrical frequency), which are caused by the signals injected into the d- and q-axis currents. The results in Figure 11b also show similar characteristics.

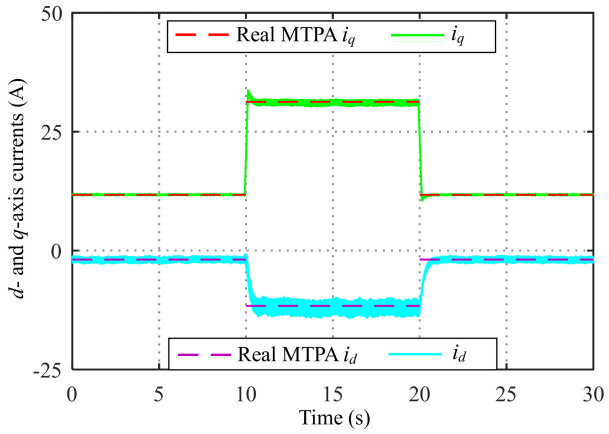


Figure 10. Experimental results of the proposed method at 500 r/min under a step torque of 10-30-10 N·m.

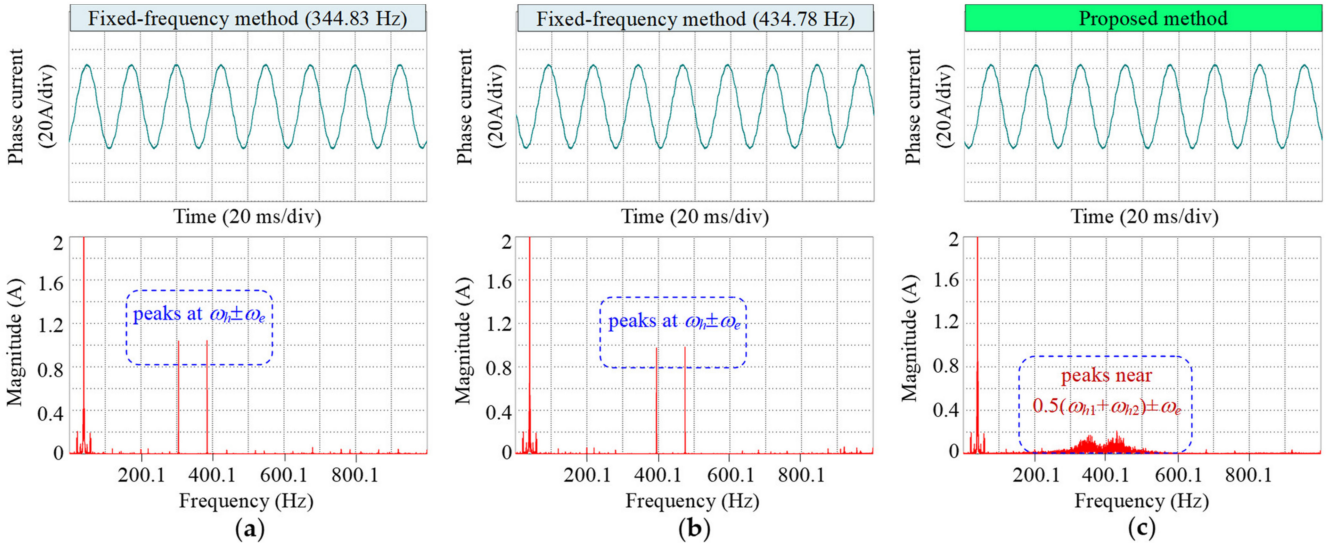


Figure 11. Stator phase currents and their FFT results of two different methods at 600 r/min under 40 N·m: (**a**) fixed-frequency method (344.83 Hz); (**b**) fixed-frequency method (434.78 Hz); (**c**) proposed PRFS method.

For the proposed method, the injection frequency switches between ω_{h1} and ω_{h2}, and the two frequencies have the same action time due to Equation (11). This implies that the mean injection frequency injected into the *d*- and *q*-axis currents is $0.5(\omega_{h1} + \omega_{h2})$. In this case, as shown in Figure 11c, the phase current FFT result of the proposed method shows two small peaks near the frequency of $0.5(\omega_{h1} + \omega_{h2}) \pm \omega_e$. It is worth noting that the injection-induced current spectrum peaks of the proposed method are significantly lower than that of the fixed-frequency method, which benefits from the randomly switching of the injection frequency. Moreover, it can be seen from Figure 11 that, unlike the fixed-frequency method whose injection-induced current spectrum is concentrated at two special frequencies, the injection-induced current spectrum of the proposed method is distributed at other frequencies in addition to two special frequencies. Since the injection-induced current spectrum of the proposed method is continuously distributed throughout a wide bandwidth (i.e., the harmonic energy is no longer concentrated) and it has very small magnitudes, the impact of the harmonic components beyond two special frequencies is negligible.

The performance of the proposed PRFS injection method and the fixed-frequency injection method were also tested under other torque levels, and the injection-induced maximum current spectrum peaks under different torque levels are summarized in Figure 12.

The results in Figure 12 show that, for any given torque level, the injection-induced maximum current spectrum peak of the proposed method is dramatically lower than that of the fixed-frequency method. Hence, the proposed method can significantly reduce the current spectrum peaks caused by the signal injection under different torque levels.

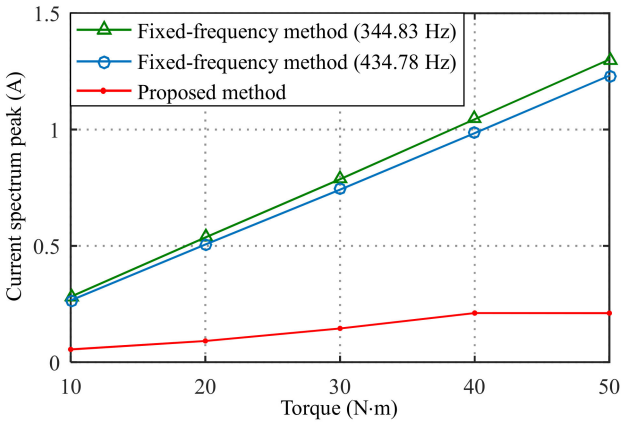


Figure 12. Injection-induced maximum current spectrum peak comparison between the proposed method and the fixed-frequency method under different torque levels.

Considering that power spectral density (PSD) is usually employed to acquire the frequency-domain characteristic of stationary random signals [29,30], the phase current of the proposed method tested at 200 r/min under 30 N·m was analyzed by means of PSD in both log and linear forms, and the results are depicted in Figure 13. The results of the fixed-frequency injection method are also depicted in Figure 13 for comparison. Because the injection frequency of the proposed method switches between ω_{h1} = 344.83 Hz and ω_{h2} = 434.78 Hz, the conventional fixed-frequency method was tested with these two injection frequencies, respectively. As can be seen from Figure 13a,b, each phase current PSD of the conventional fixed-frequency method consists of two discrete spectra at the frequency of $\omega_h \pm \omega_e$, which are induced by the signal injection. By contrast, the phase current PSD of the proposed method shown in Figure 13c contains some continuous spectra near the frequency of $0.5(\omega_{h1} + \omega_{h2}) \pm \omega_e$ instead of two discrete spectra. In addition, it can be seen that the spectrum peaks in the linear PSD of the proposed method are less than 2.64% of that of the fixed-frequency method. Hence, with the proposed method, the injection-induced current spectrum peaks are significantly reduced.

For intuitive comparison, Figure 14 shows the injection-induced maximum current spectrum peak in PSD of the proposed method and that of the fixed-frequency method under different torque levels. In Figure 14a,b, the PSDs are presented in log and linear forms, respectively. It can be seen from Figure 14 that for any given torque level, the proposed method exhibits a very lower injection-induced current spectrum peak in PSD than the fixed-frequency method. Therefore, the characteristic that the proposed method has a significant current spectrum peak reduction effect is also confirmed from the PSD point of view.

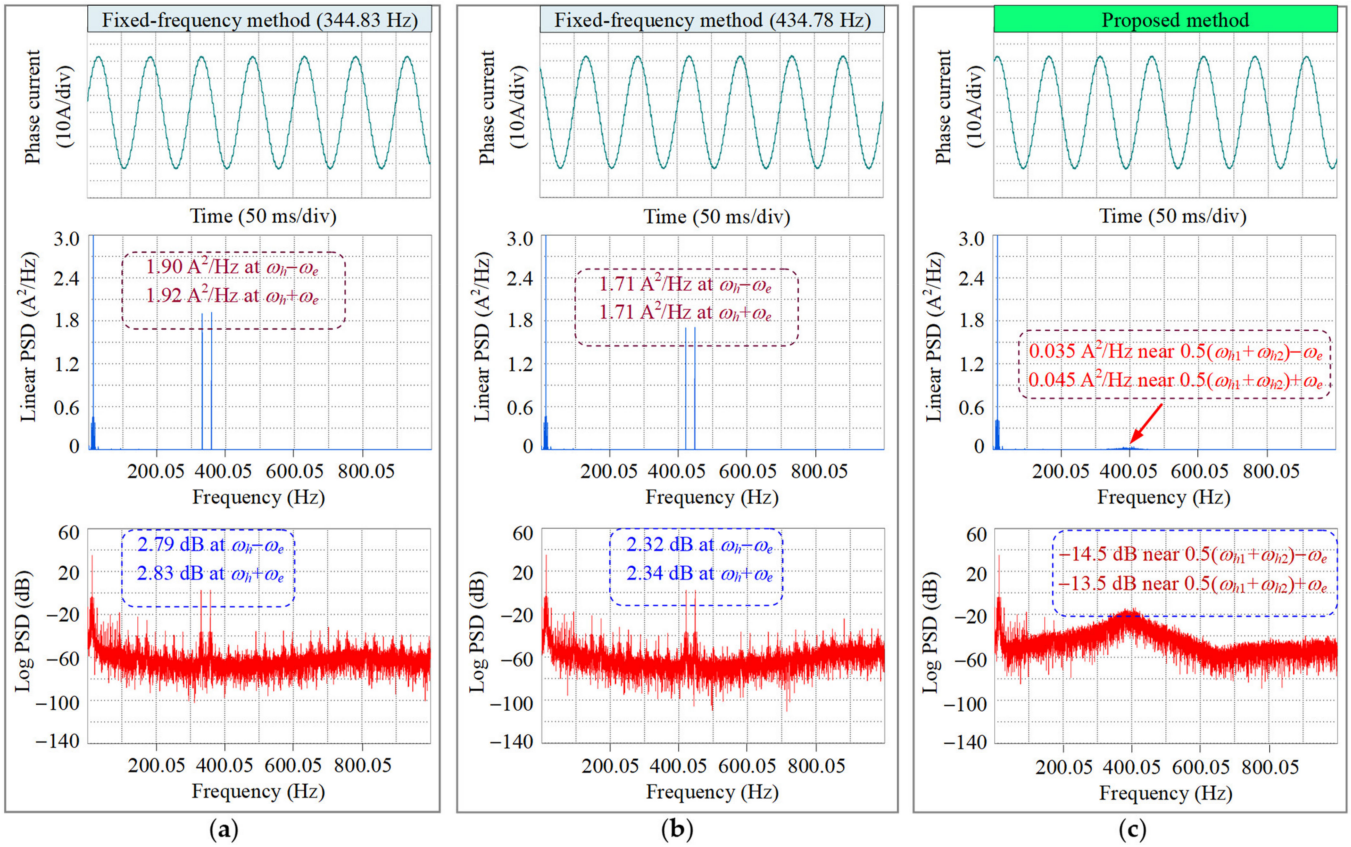


Figure 13. Stator phase currents and their PSD results of two different methods at 200 r/min under 30 N·m: (**a**) fixed-frequency method (344.83 Hz); (**b**) fixed-frequency method (434.78 Hz); (**c**) proposed PRFS method.

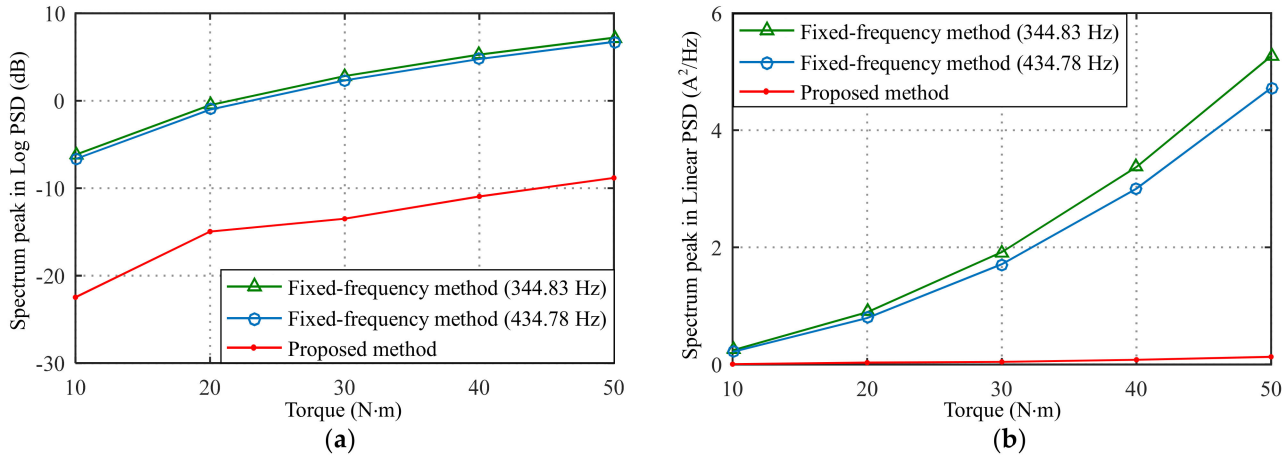


Figure 14. Comparison between the proposed method and the fixed-frequency method in terms of injection-induced maximum current spectrum peak in: (**a**) log PSD; (**b**) linear PSD.

5. Conclusions

This paper has proposed an MTPA control scheme based on PRFS sinusoidal signal injection for IPMSM drives. This method is insensitive to motor parameter variations and can realize a high-performance MTPA control. Different from the conventional fixed-frequency signal injection methods, the presented method employs the randomly switching injection frequency. Therefore, the induced HF components in phase currents no longer concentrate at certain frequencies, and the current spectrum peaks caused by signal injection can be significantly reduced accordingly. This characteristic is beneficial for the proposed

method to be applied to more applications. The effectiveness of the presented method has been experimentally confirmed based on a prototype IPMSM drive system. The results have shown that, taking 40 N·m torque level as an example, the injection-induced maximum current spectrum peak of the proposed method can be reduced to a quantity less than 21.6% of that of the fixed-frequency method, and its injection-induced maximum current spectrum peak in linear PSD can be reduced to a quantity less than 2.68% of that of the fixed-frequency method. Additionally, under severe conditions, both the simulation and experimental results have validated the stability of the proposed method.

Author Contributions: Conceptualization, K.L., T.S., W.F. and H.L.; methodology, K.L. and T.S.; software, K.L. and F.J.; validation, K.L. and T.S.; formal analysis, K.L., T.S. and F.J.; investigation, K.L. and F.J.; resources, T.S., W.F. and H.L.; data curation, T.S.; writing—original draft preparation, K.L.; writing—review and editing, K.L. and T.S.; visualization, K.L. and F.J.; supervision, T.S., W.F. and H.L.; project administration, T.S. and W.F.; funding acquisition, T.S., W.F. and H.L. All authors have read and agreed to the published version of the manuscript.

Funding: This research was partly funded by Key-Area R&D Program of Guangdong Province, 2020B090925002 and 2019B090917001, the National Natural Science Foundation of China (NSFC), 51707191, the Shenzhen Science and Technology Program, JSGG20210629144805018, JCYJ20180507182619669, JCYJ20200109115414354 and JCYJ20200109115403807, and the Youth Innovation Promotion Association of the Chinese Academy of Sciences, 2021360.

Institutional Review Board Statement: Not applicable.

Informed Consent Statement: Not applicable.

Data Availability Statement: Not applicable.

Acknowledgments: The authors would like to thank the support from Shenzhen Key Laboratory of Electric Vehicle Powertrain Platform and Safety Technology.

Conflicts of Interest: The authors declare no conflict of interest.

References

1. Wang, C.S.; Guo, C.W.C.; Tsay, D.M.; Perng, J.W. PMSM Speed Control Based on Particle Swarm Optimization and Deep Deterministic Policy Gradient under Load Disturbance. *Machines* **2021**, *9*, 343. [CrossRef]
2. Hezzi, A.; Elghali, S.B.; Bensalem, Y.; Zhou, Z.; Benbouzid, M.; Abdelkrim, M.N. ADRC-Based Robust and Resilient Control of a 5-Phase PMSM Driven Electric Vehicle. *Machines* **2020**, *8*, 17. [CrossRef]
3. Ni, R.; Xu, D.; Wang, G.; Li, D.; Zhang, G.; Qu, L. Maximum Efficiency per Ampere Control of Permanent-Magnet Synchronous Machines. *IEEE Trans. Ind. Electron.* **2015**, *62*, 2135–2143. [CrossRef]
4. Hang, J.; Wu, H.; Ding, S.; Huang, Y.; Hua, W. Improved Loss Minimization Control for IPMSM Using Equivalent Conversion Method. *IEEE Trans. Power Electron.* **2021**, *36*, 1931–1940. [CrossRef]
5. Sun, J.; Lin, C.; Xing, J.; Jiang, X. Online MTPA Trajectory Tracking of IPMSM Based on a Novel Torque Control Strategy. *Energies* **2019**, *12*, 3261. [CrossRef]
6. Dianov, A.; Tinazzi, F.; Calligaro, S.; Bolognani, S. Review and Classification of MTPA Control Algorithms for Synchronous Motors. *IEEE Trans. Power Electron.* **2022**, *37*, 3990–4007. [CrossRef]
7. Lin, F.J.; Liao, Y.H.; Lin, J.R.; Lin, W.T. Interior Permanent Magnet Synchronous Motor Drive System with Machine Learning-Based Maximum Torque per Ampere and Flux-Weakening Control. *Energies* **2021**, *14*, 346. [CrossRef]
8. Cao, M.; Egashira, J.; Kaneko, K. High Efficiency Control of IPMSM for Electric Motorcycles. In Proceedings of the IEEE 6th International Power Electronics and Motion Control Conference (IPEMC), Wuhan, China, 17–20 May 2009.
9. Wang, G.; Li, Z.; Zhang, G.; Yu, Y.; Xu, D. Quadrature PLL-Based High-Order Sliding-Mode Observer for IPMSM Sensorless Control with Online MTPA Control Strategy. *IEEE Trans. Energy Convers.* **2013**, *28*, 214–224. [CrossRef]
10. Xia, Z.; Nalakath, S.; Tarvirdilu Asl, R.; Sun, Y.; Wiseman, J.; Emadi, A. Online Optimal Tracking Method for Interior Permanent Magnet Machines with Improved MTPA and MTPV in Whole Speed and Torque Ranges. *IEEE Trans. Power Electron.* **2020**, *35*, 9753–9769. [CrossRef]
11. Shinohara, A.; Inoue, Y.; Morimoto, S.; Sanada, M. Direct Calculation Method of Reference Flux Linkage for Maximum Torque per Ampere Control in DTC-Based IPMSM Drives. *IEEE Trans. Power Electron.* **2017**, *32*, 2114–2122. [CrossRef]
12. Jung, S.Y.; Hong, J.; Nam, K. Current Minimizing Torque Control of the IPMSM Using Ferrari's Method. *IEEE Trans. Power Electron.* **2013**, *28*, 5603–5617. [CrossRef]
13. Mohamed, Y.A.R.I.; Lee, T.K. Adaptive Self-Tuning MTPA Vector Controller for IPMSM Drive System. *IEEE Trans. Energy Convers.* **2006**, *21*, 636–644. [CrossRef]

14. Sun, T.; Koc, M.; Wang, J. MTPA Control of IPMSM Drives Based on Virtual Signal Injection Considering Machine Parameter Variations. *IEEE Trans. Ind. Electron.* **2018**, *65*, 6089–6098. [CrossRef]
15. Li, K.; Wang, Y. Maximum Torque per Ampere (MTPA) Control for IPMSM Drives Based on a Variable-Equivalent-Parameter MTPA Control Law. *IEEE Trans. Power Electron.* **2019**, *34*, 7092–7102. [CrossRef]
16. Bolognani, S.; Petrella, R.; Prearo, A.; Sgarbossa, L. Automatic Tracking of MTPA Trajectory in IPM Motor Drives Based on AC Current Injection. *IEEE Trans. Ind. Appl.* **2011**, *47*, 105–114. [CrossRef]
17. Lai, C.; Feng, G.; Mukherjee, K.; Tjong, J.; Kar, N.C. Maximum Torque per Ampere Control for IPMSM Using Gradient Descent Algorithm Based on Measured Speed Harmonics. *IEEE Trans. Ind. Inform.* **2018**, *14*, 1424–1435. [CrossRef]
18. Antonello, R.; Carraro, M.; Zigliotto, M. Maximum-Torque-per-Ampere Operation of Anisotropic Synchronous Permanent-Magnet Motors Based on Extremum Seeking Control. *IEEE Trans. Ind. Electron.* **2014**, *61*, 5086–5093. [CrossRef]
19. Kim, S.; Yoon, Y.D.; Sul, S.K.; Ide, K. Maximum Torque per Ampere (MTPA) Control of an IPM Machine Based on Signal Injection Considering Inductance Saturation. *IEEE Trans. Power Electron.* **2013**, *28*, 488–497. [CrossRef]
20. Liu, G.; Wang, J.; Zhao, W.; Chen, Q. A Novel MTPA Control Strategy for IPMSM Drives by Space Vector Signal Injection. *IEEE Trans. Ind. Electron.* **2017**, *64*, 9243–9252. [CrossRef]
21. Li, K.; Wang, Y. Maximum Torque per Ampere (MTPA) Control for IPMSM Drives Using Signal Injection and an MTPA Control Law. *IEEE Trans. Ind. Inform.* **2019**, *15*, 5588–5598. [CrossRef]
22. Wang, G.; Zhou, H.; Zhao, N.; Li, C.; Xu, D. Sensorless Control of IPMSM Drives Using a Pseudo-Random Phase-Switching Fixed-Frequency Signal Injection Scheme. *IEEE Trans. Ind. Electron.* **2018**, *65*, 7660–7671. [CrossRef]
23. Sun, T.; Wang, J.; Chen, X. Maximum Torque per Ampere (MTPA) Control for Interior Permanent Magnet Synchronous Machine Drives Based on Virtual Signal Injection. *IEEE Trans. Power Electron.* **2015**, *30*, 5036–5045. [CrossRef]
24. Sun, T.; Wang, J.; Koc, M. Self-Learning Direct Flux Vector Control of Interior Permanent-Magnet Machine Drives. *IEEE Trans. Power Electron.* **2017**, *32*, 4652–4662. [CrossRef]
25. Wang, J.; Huang, X.; Yu, D.; Chen, Y.; Zhang, J.; Niu, F.; Fang, Y.; Cao, W.; Zhang, H. An Accurate Virtual Signal Injection Control of MTPA for an IPMSM with Fast Dynamic Response. *IEEE Trans. Power Electron.* **2018**, *33*, 7916–7926. [CrossRef]
26. Chen, Q.; Zhao, W.; Liu, G.; Lin, Z. Extension of Virtual-Signal-Injection-Based MTPA Control for Five-Phase IPMSM into Fault-Tolerant Operation. *IEEE Trans. Ind. Electron.* **2019**, *66*, 944–955. [CrossRef]
27. Sun, T.; Long, L.; Yang, R.; Li, K.; Liang, J. Extended Virtual Signal Injection Control for MTPA Operation of IPMSM Drives with Online Derivative Term Estimation. *IEEE Trans. Power Electron.* **2021**, *36*, 10602–10611. [CrossRef]
28. Marsaglia, G. Xorshift RNGs. *J. Stat. Softw.* **2003**, *8*, 1–6. [CrossRef]
29. Zhang, G.; Xiang, R.; Wang, G.; Li, C.; Bi, G.; Zhao, N.; Xu, D. Hybrid Pseudorandom Signal Injection for Position Sensorless SynRM Drives with Acoustic Noise Reduction. *IEEE Trans. Transport. Electrif.* **2021**, *in press*. [CrossRef]
30. Li, C.; Wang, G.; Zhang, G.; Zhao, N.; Xu, D. Adaptive Pseudorandom High-Frequency Square-Wave Voltage Injection Based Sensorless Control for SynRM Drives. *IEEE Trans. Power Electron.* **2021**, *36*, 3200–3210. [CrossRef]